

Two-step combustion synthesis of nanocrystalline $\text{Zn}_{1-x}\text{Mn}_x\text{Fe}_2\text{O}_4$ ($0 \leq x \leq 1$) spinel ferrites with linear tuning of magnetic parameters

K. D. Martinson, V. I. Popkov

Ioffe Institute, St. Petersburg, 194021, Russia

martinsonkirill@mail.ru

PACS 61.46.+w, 75.50.Bb, 75.60.-d

DOI 10.17586/2220-8054-2021-12-5-634-640

Multicomponent zinc ferrites are of great applied value due to their functional features, due to which they are widely used in the production of microwave devices. In this regard, the development of new methods for obtaining initial pre-ceramic nanopowders in a nanostructured form is especially urgent. In this work, multicomponent zinc-manganese ferrites of the $\text{Zn}_{1-x}\text{Mn}_x\text{Fe}_2\text{O}_4$ ($x = 0, 0.2, \dots, 1.0$) composition were obtained by thermal treatment of X-ray amorphous products of solution combustion synthesis at a temperature of 750 °C and a holding time of 6 hours. The synthesized powders were analyzed by PXRD, FT-IR, and SEM methods. The magnetic characteristics were determined by vibration magnetometry. It was shown that the obtained samples contain one-phase spinel ferrite without any noticeable impurities. Depending on the number of Mn^{2+} cations in the crystal lattice, the unit cell parameters varied from 8.485(2) to 8.451(2) Å. The average crystallite size of the powders varied from 29.4 nm in the case of zinc ferrite to 36.8 nm in the case of MnFe_2O_4 . Residual magnetization (M_s), saturation magnetization (M_T), and coercive force (H_c) also depend on the content of manganese cations in spinel and varied from 4.9 to 12.3 emu/g, from 22.4 to 76.4 emu/g, and from 47.5 to 81.3 Oe, respectively and these dependencies are almost linear. The highest magnetic parameters were found in simple manganese ferrite, which has the largest crystallite size.

Keywords: zinc-manganese ferrite, solution combustion, nanocrystals, structure transformation, magnetic properties.

Received: 25 August 2021

Revised: 14 September 2021

1. Introduction

Ferrites are well-known spinel compounds with the general formula MFe_2O_4 ($\text{M} = \text{Co}, \text{Ni}, \text{Zn}, \text{Mn}, \text{et al.}$). The peculiarities of their functional behavior are associated with their structural features, namely the cubic system, which contains 32 oxygen anions occupying 8 regions (4 anions in each), 8 M^{2+} cations (one cation each in 8 regions), and 16 Fe^{3+} cations (two cations each in 8 regions) [1]. The unique magnetic properties of ferrites arise primarily due to a divalent transition metal cation introduced into the crystal structure, which occupies the tetrahedral position (A) in the case of normal spinel and the octahedral position (B) in the case of inverted spinel [2]. Inverted spinels are a more complex structural unit in this case, since the M^{2+} cation can replace both the A and B positions. Such spinels are called mixed and their magnetic behavior can change significantly depending on composition and structural features [3].

Multicomponent zinc ferrites correspond to the structure of normal spinel in which the Zn^{2+} cation occupies a tetrahedral position, while the Fe^{3+} cations are located in the octahedral regions. The magnetic behavior of zinc ferrite is based on its antiferrimagnetic nature, which is characterized by a weak super exchange interaction due to an angle of 90° in the $\text{Fe}^{3+}-\text{O}-\text{Fe}^{3+}$ bond [4]. In the case of multicomponent zinc ferrites, cations of transition metals, including Mn^{2+} , Co^{2+} , Ni^{2+} , etc., most often act as an alloying addition [5, 6]. In particular, zinc-manganese ferrites should be highlighted, which have found wide application in the field of microwave technology [7], in the production of magnetic fluids [8], as contrast agents for magnetic resonance imaging [9], for drug delivery [10], etc. In addition, several works have shown the possibility of using nanostructured spinel ferrites as catalysts and photocatalysts [11], for wastewater treatment [12], as antibacterial materials [13]. For the application of this class of compounds in these areas, structural parameters are especially important, among which the size of particles and their size distribution should be singled out separately [14]. In recent years, a large number of methods have been used to obtain ferrite nanopowders of various compositions, including hydrothermal synthesis [15], co-precipitation method [16], solution combustion method [17], sol-gel synthesis [18], and many other methods. Each of these types of synthesis has its advantages and disadvantages, but from the point of view of possible industrial scale-up, various methods of solution combustion are of particular interest [19, 20]. They are most often based on the preparation of a homogeneous solution, which contains cations of the corresponding metals and organic fuel acting as a chelating agent and initiator of the combustion process [21]. Since the combustion process is completed within a few seconds, and the initial reagents are dissolved in the solution, its use makes it possible to obtain nanoparticles with controlled functional characteristics in a wide range of particle

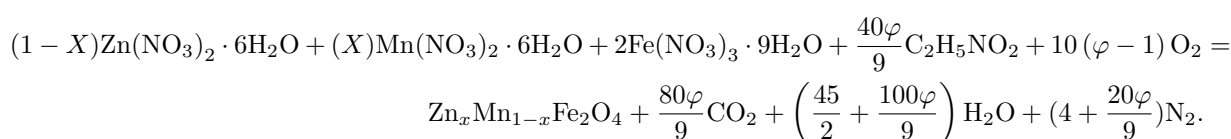
sizes [22–24]. Nevertheless, this technique has some disadvantages, among which is the difficulty of obtaining some complex oxide systems without impurities [25] and the difficulty in obtaining particles less than 30 nm in size.

In this regard, the search for modified multistage methods of solution combustion with a wider set of controlled synthesis parameters, due to which it is possible to obtain pure multicomponent phases with small particle size, becomes especially urgent. One of these methods is the method of thermal treatment of X-ray amorphous products of solution combustion, within which the initial powder is synthesized with a significant excess or shortage of fuel and is thermally treated in an air atmosphere at temperatures from 500 to 800 °C. This original technique was first applied by the authors of this work for the synthesis of holmium and europium orthoferrites [26, 27]. Nevertheless, the question of whether it can be used to obtain multicomponent spinel ferrites remains unanswered.

In this article, the method of thermal treatment of X-ray amorphous products of solution combustion was applied to obtain single-phase nanostructured powders of the composition $Zn_{1-x}Mn_xFe_2O_4$ ($x = 0, 0.2, \dots, 1.0$) with a particle size of up to 29 nm. The starting powders were synthesized under the conditions of glycine-nitrate combustion with a significant lack of organic fuel. The samples obtained were thermally treated under aerobic conditions at 750 °C for 6 hours and studied using a complex of physicochemical methods of analysis.

2. Experimental

The synthesis of nanopowders of zinc-manganese ferrites of the $Zn_{1-x}Mn_xFe_2O_4$ ($x = 0, 0.2, \dots, 1.0$) composition was carried out in two stages. At the first stage, the initial powder was obtained by the method of solution combustion with the addition of a small amount of glycine (redox ratio = 0.2). The following compounds were chosen as the starting reagents for the synthesis: $Zn(NO_3)_2 \cdot 6H_2O$ (puriss., NevaReactiv), $Mn(NO_3)_2 \cdot 6H_2O$ (puriss., NevaReactiv), $Fe(NO_3)_3 \cdot 9H_2O$ (puriss., NevaReactiv), CH_2NH_2COOH (puriss., NevaReactiv) and distilled water. The reagents were dissolved in 50 ml of distilled water with constant mechanical stirring and then heated until the water was almost completely removed and the autoignition process began, during which solid and gaseous reaction products were formed. The weighed portions were taken taking into account the reaction of the formation of the final product ($x = 0, 0.2, \dots, 1.0$):



During the second stage of the synthesis, the powders thus obtained were mechanically ground in a mortar and thermally treated aerobically at 750 °C for 6 hours.

The phase composition of the synthesized samples was studied by powder X-ray diffractometry (PXRD) using $CuK\alpha$ radiation ($\lambda = 0.15406$ nm) on a RigakuSmartLab 3 X-ray diffractometer. The obtained diffractograms were processed in the RigakuSmartLab Studio II software package and using the ICDD PDF 2 powder database. The average crystallite size was calculated using the Scherrer formula, and the crystallite size distribution was constructed using the method of fundamental parameters. The unit cell parameters were determined using the Rietveld method. A Shimadzu IRTracer-100 FT-IR spectrometer was used to obtain infrared spectra (FT-IR) in the wavenumbers ranging from 400 to 1600 cm^{-1} . The morphology and elemental analysis of the synthesized powders were determined by scanning electron microscopy (SEM) and energy dispersive analysis (EDX) using a Tescan Vega 3 SBH electron microscope equipped with an Oxford INCA x-act X-ray spectral microanalysis attachment. Magnetic hysteresis loops were obtained using a LakeShore 7410 vibrating magnetometer in an external magnetic field ranging from –4000 to 4000 Oe.

3. Results and discussion

Diffraction patterns of the synthesized samples of zinc-manganese ferrites of the composition $Zn_{1-x}Mn_xFe_2O_4$ ($x = 0, 0.2, \dots, 1.0$) are shown in Fig. 1. The data obtained indicate that all the obtained powders contain one phase – ferrite of the corresponding composition.

Large values of the line width of the diffraction maxima indicate the nanoscale nature of the obtained crystallites. Refinement of the diffraction patterns performed by the Rietveld method indicates that all samples correspond to the space group $Fd3m$ and contain up to 95 – 97 % of the crystalline phase and from 3 to 5 % of the amorphous phase. With a change in the number of Mn^{2+} cations in the lattice, the diffraction peaks shift, which is clearly shown in Fig. 1b. In the crystallographic direction (111) using the method of fundamental parameters, the size distribution of crystallites was calculated (Fig. 2), which indicates that a narrow distribution is observed in all samples, which is virtually identical in appearance. It is characteristic that the narrowest is the distribution for simple zinc ferrite, while the synthesized $MnFe_2O_4$ nanopowder has a somewhat wider distribution. This may be due to the peculiarities of the

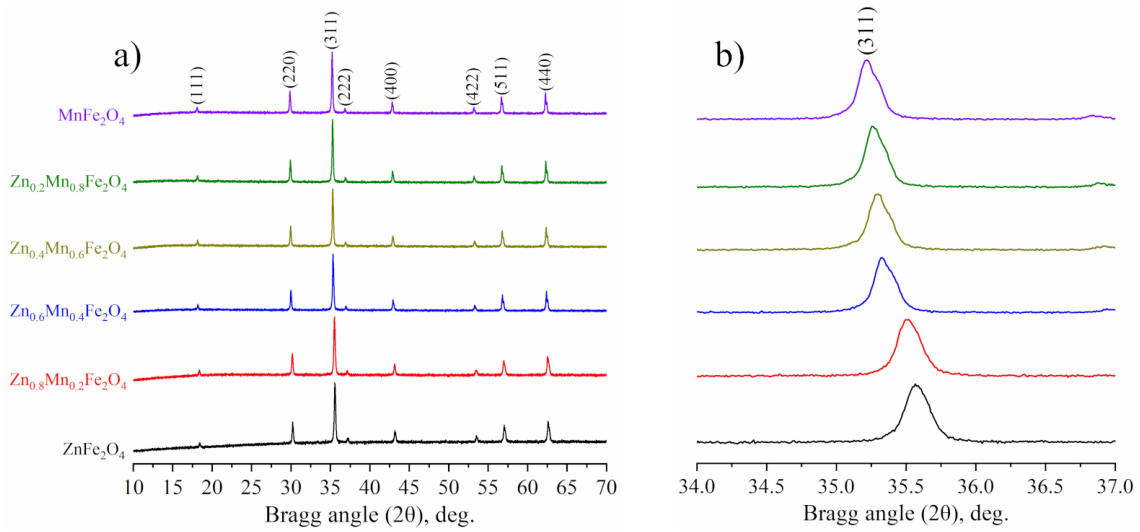


FIG. 1. Survey (a) and local (b) PXRD patterns of the synthesized $Zn_xMn_{1-x}Fe_2O_4$ nanopowders

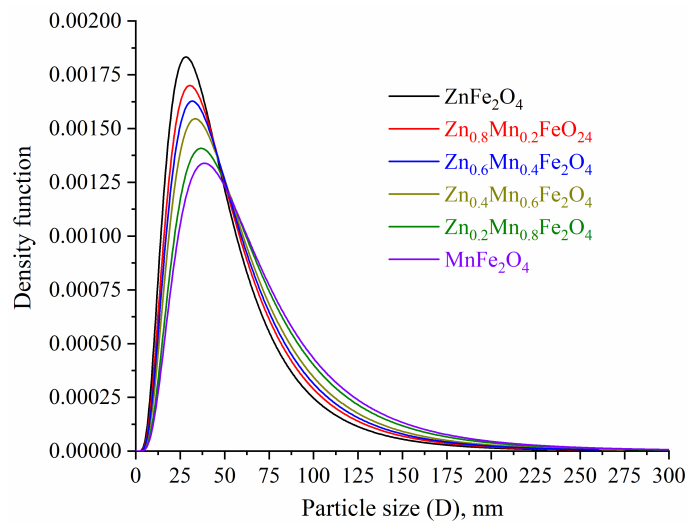


FIG. 2. Lognormal size distribution of the synthesized Zn–Mn ferrite nanocrystals

processes of ferrite formation under conditions of solution combustion and a change in temperature in the combustion front, depending on the chemical composition of the reaction medium [28].

The obtained data for the size distribution of crystallites are in good agreement with the calculations for the average crystallite size according to the Scherrer formula (Fig. 3). It was shown that, in the case of $ZnFe_2O_4$, crystallites with the smallest size (~ 29.4 nm) are formed, while in the case of manganese ferrite, the average crystallite size is somewhat larger and equal to 36.8 nm. It is noteworthy that with a change in the fraction of manganese cations in a multicomponent ferrite, the average crystallite size changes monotonically from larger ($MnFe_2O_4$) to smaller ($ZnFe_2O_4$). This indirectly confirms the effect on the crystallite size of the composition of the initial reaction medium and, as a consequence, the conditions of the combustion reaction.

In addition, using the Rietveld method, the unit cell parameters were calculated, the results of which are shown in Fig. 3b. The data obtained indicate that with an increase in the dopant, Mn^{2+} leads to a decrease in the lattice constant from 8.485(2) for $ZnFe_2O_4$ to 8.451(2) for $MnFe_2O_4$. This is because Mn^{2+} cations have a larger ionic radius (0.082 nm) compared to Zn^{2+} cations (0.074 nm). Separately, it should be noted that in mixed Zn–Mn ferrite, manganese cations are usually randomly distributed at tetrahedral positions (A) and octahedral positions (B), while zinc cations are usually located only in tetrahedral regions (A) [29]. This explains why, in the case of zinc ferrite and

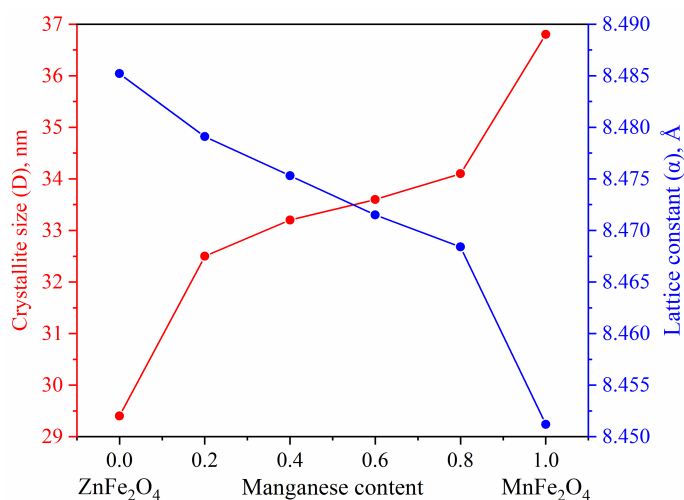


FIG. 3. Average crystallite sizes and lattice constants depending on the Mn content in Zn–Mn ferrites

mixed Zn–Mn ferrite, the change in the lattice constant proceeds linearly, while between the $Zn_{0.2}Mn_{0.8}Fe_2O_4$ and $MnFe_2O_4$ samples there is a significant change in the parameter α .

The FT-IR spectra of all synthesized samples (Fig. 4) show only two main absorption bands in the range of $605 - 404 \text{ cm}^{-1}$. The absence of bending and stretching vibrations related to O–H, C=O bonds, etc., indirectly indicated the complete formation of Zn–Mn ferrites at a temperature of $750 \text{ }^\circ\text{C}$. The set of absorption bands in the range from 568 to 605 cm^{-1} referred to the stretching vibrations of oxygen in the M–O–Fe (M–Zn, Mn) and Fe–O–Fe systems [30].

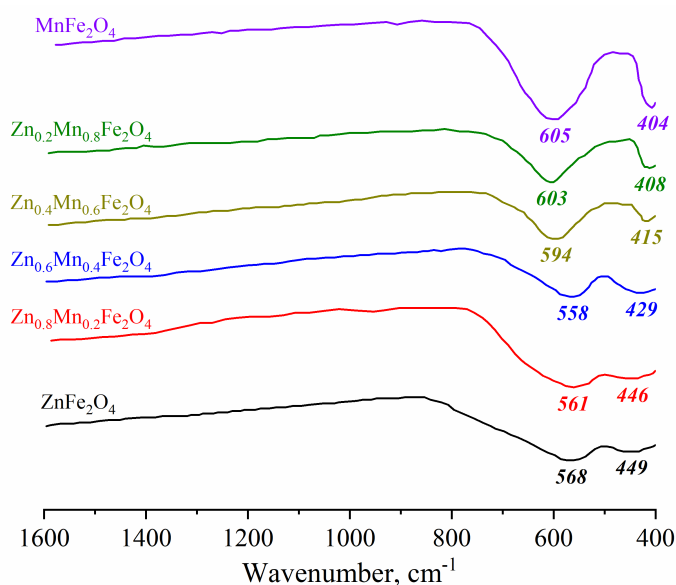


FIG. 4. FT-IR spectra of the obtained $Zn_{1-x}Mn_xFe_2O_4$ ferrites

In turn, absorption bands from 404 to 449 cm^{-1} indicated the presence of bending O–Fe–O vibrations in the synthesized samples [31]. The described two types of vibrations are characteristic of spinel ferrites and their presence in the resulting powders confirmed the successful formation of zinc-manganese ferrites. It should be noted separately that, depending on the composition, there is a slight shift of the absorption bands. As in the case of the diffraction results, this is due to a change in the fraction of manganese cations in the crystal lattice.

Figure 5 shows the results of studying the morphology of synthesized samples of zinc-manganese ferrites of various compositions. The results obtained indicate that simple zinc and manganese ferrites have a typical morphology of solid solution combustion products, which is characteristic of spinel ferrites synthesized by this technique. The most remarkable are samples of mixed Zn–Mn ferrites in which nanoparticles are collected in submicron agglomerates lying

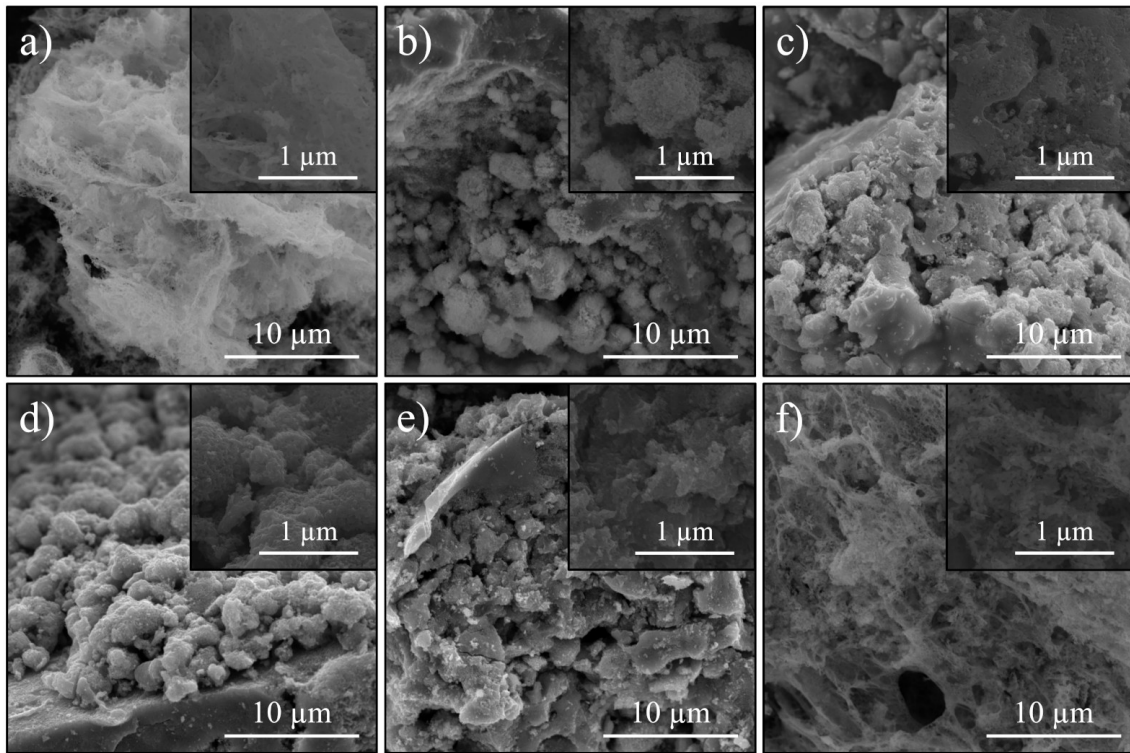


FIG. 5. SEM images of the Zn–Mn ferrite powders synthesized via heat treatment of amorphous combustion products

on the surface of larger irregularly shaped agglomerations several tens of microns in size. In the insets in Fig. 5(b, c and d), you can see the effects of the thermal treatment process, during which the particles are sintered together. According to the elemental analysis data, all synthesized compositions corresponded in their experimental composition to the calculated composition within the experimental error of the determination method.

Magnetic M–H loops of the obtained powders were constructed using a vibration magnetometer and are shown in Fig. 6. According to the presented data, the content of manganese cations significantly changes the magnetic behavior of multicomponent zinc ferrite nanopowders. It is easy to see that the change in the hysteresis loops is linear and their appearance changes significantly in the series $\text{ZnFe}_2\text{O}_4\text{--Zn}_{1-x}\text{Mn}_x\text{Fe}_2\text{O}_4\text{--MnFe}_2\text{O}_4$. As mentioned above, this is due to both the peculiarities of the magnetic behavior of simple zinc and manganese ferrites (which are normal spinels) and mixed Zn–Mn ferrites and the peculiarities of the distribution of Zn^{2+} and Mn^{2+} cations in their lattice.

The largest values of the main magnetic parameters (remanent magnetization, saturation magnetization, and coercive force) were observed in the case of simple zinc ferrite and were 4.9 emu/g, 22/4 emu/g, and 47.5 Oe, respectively (Fig. 7). On the contrary, MnFe_2O_4 nanoparticles exhibited the most pronounced magnetic characteristics ($M_r = 12.3$ emu/g, $M_s = 76.4$ emu/g, $H_c = 81.3$ Oe). The data obtained indicated that an increase in the proportion of manganese cations was accompanied by a linear increase in magnetic characteristics. This is due to the structural features of the obtained powders. It is known that spinel ferrites have three types of magnetic interaction: between metal cations located at tetrahedral positions (A–A), between metal cations located at octahedral positions (B–B), and between metal cations located in both of these regions (A–B). With an increase in the proportion of manganese in spinel, it replaces the Fe^{3+} cations at octahedral and tetrahedral positions, thereby changing the nature of the magnetic behavior of mixed ferrites.

4. Conclusion

Thus, in this work, for the first time, an original method was proposed for obtaining nanoparticles of multicomponent zinc-manganese ferrites of the composition $\text{Zn}_{1-x}\text{Mn}_x\text{Fe}_2\text{O}_4$ ($x = 0, 0.2, \dots, 1.0$) by thermal treatment of X-ray amorphous combustion products. The use of this technique made it possible to obtain nanoparticles in sizes ranging from 29.4 to 36.8 nm with high values of remanent magnetization ($M_r = 4.9 - 12.3$ emu/g), saturation

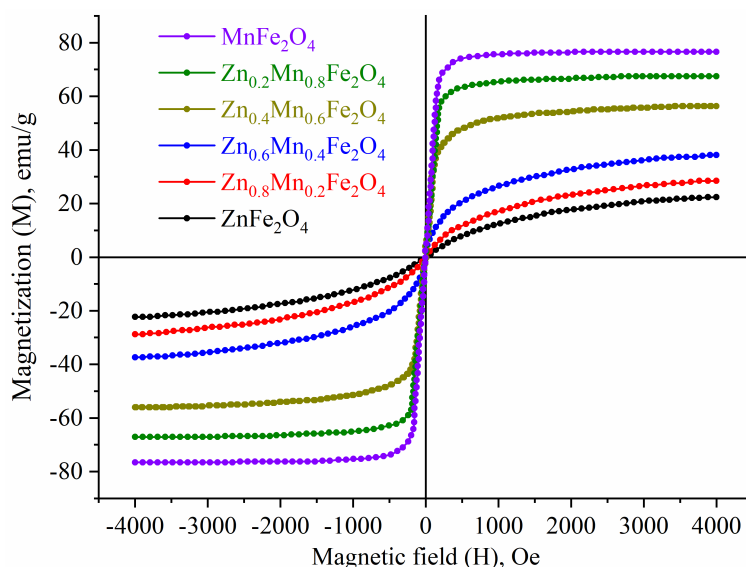


FIG. 6. M–H loops of Mn–Zn ferrite nanopowders at a room temperature

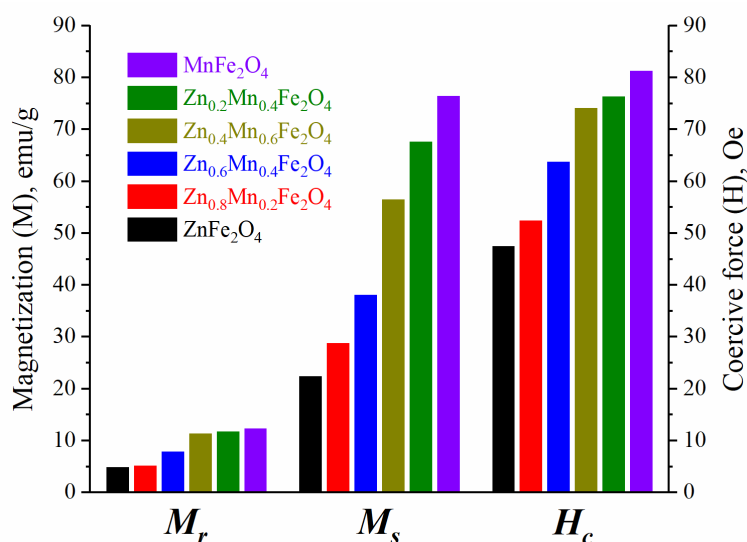


FIG. 7. The main magnetic parameters of the obtained zinc-manganese ferrites of various compositions

magnetization ($M_s = 22.4 - 76.4$ emu/g) and coercive force ($H_c = 47.5 - 81.3$ Oe). The absence of extraneous impurity phases suggests that this synthesis method is promising for obtaining pure multicomponent ferrites of various compositions and linearly tunable magnetic characteristics.

Acknowledgements

The reported study was funded by RFBR, project number 20-03-00976.

References

- [1] Narang S.B., Pubby K. Nickel spinel ferrites: a review. *Journal of Magnetism and Magnetic Materials*, 2021, **519**, 167163.
- [2] Varshney D., Verma K., Kumar A. Structural and vibrational properties of $Zn_xMn_{1-x}Fe_2O_4$ ($x = 0.0, 0.25, 0.50, 0.75, 1.0$) mixed ferrites. *Materials Chemistry and Physics*, 2011, **131**, P. 413-419.
- [3] Martinson K.D., Ivanov A.A., Panteleev I.B., Popkov V.I. Effect of sintering temperature on the synthesis of LiZnMnFe microwave ceramics with controllable electro/magnetic properties. *Ceramics International*, 2021, **47**, P. 30071–30081.
- [4] Hwang J., Choi M., et al. Structural and magnetic properties of NiZn ferrite nanoparticles synthesized by a thermal decomposition method. *Applied Sciences*, 2020, **10**, 6279.

- [5] Msomi J.Z., Nhlapo T.A., et al. Grain size effects on the magnetic properties of $Zn_xMn_{1-x}Fe_2O_4$ nanoferrites. *Journal of Magnetism and Magnetic Materials*, 2015, **373**, P. 74–77.
- [6] Azouaoui A., Haoua M.E., et al. Structural and magnetic properties of Co–Zn ferrites: density functional theory calculations and high-temperature series expansions. *Computational Condensed Matter*, 2020, **23**, 00454.
- [7] Praveena K., Sadhana K., Bharadwaj S., Murthy S.R. Development of nanocrystalline Mn–Zn ferrites for high frequency transformer applications. *J. of Magnetism and Magnetic Materials*, 2009, **321**, P. 2433–2437.
- [8] Dyachenko S.V., Vasishenkova M.A., et al. Synthesis and properties of magnetic fluids produced on the basis of magnetite particles. *Russian J. of Applied Chemistry*, 2016, **89**, P. 690–696.
- [9] Nandwana V., Zhou R., et al. Exchange coupling in soft magnetic nanostructures and its direct effect on their theranostic properties. *ACS Applied Materials & Interfaces*, 2018, **10**, P. 27233–27243.
- [10] Cojocariu A.M., Doaga A., et al. Synthesis and functionalization of magnetic nanoparticles with possible application in drug delivery systems. *Digest J. of Nanomaterials and Biostructures*, 2013, **8**, P. 519–527.
- [11] Tikhanova S.M., Lebedev L.A., et al. The synthesis of novel heterojunction h-YbFeO₃/o-YbFeO₃ photocatalyst with enhanced Fenton-like activity under visible-light. *New J. of Chemistry*, 2021, **45**, P. 1541–1550.
- [12] Kefeni K.K., Mamba B.B., Msagati T.A.M. Application of spinel ferrite nanoparticles in water and wastewater treatment: a review. *Separation and Purification Technology*, 2017, **188**, P. 399–422.
- [13] Haghniaz R., Rabbani A., et al. Anti-bacterial and wound healing-promoting effects of zinc ferrite nanoparticles. *J. of Nanobiotechnology*, 2021, **19**, 38.
- [14] Martinson K.D., Pantelev I.B., Shevchik A.P., Popkov V.I. Effect on the Red/Ox ratio on the structure and magnetic behavior of $Li_{0.5}Fe_{2.5}O_4$ nanocrystals synthesized by solution combustion approach. *Letters on Materials*, 2019, **9**, P. 475–479.
- [15] Hu X., Guan P., Yan X. Hydrothermal synthesis of nano-meter microporous zinc ferrite. *China Particuology*, 2004, **2**, P. 135–137.
- [16] Mello L.B., Varanda L.C., Sigoli F.A., Mazali I.O. Co-precipitation synthesis of (Zn–Mn)-co-doped magnetite nanoparticles and their application in magnetic hyperthermia. *J. of Alloys and Compounds*, 2019, **779**, P. 698–705.
- [17] Martinson K.D., Ivanov V.A., et al. Facile combustion synthesis of TbFeO₃ nanocrystals with hexagonal and orthorhombic structure. *Nanosystems: Physics, Chemistry, Mathematics*, 2019, **10**, P. 694–700.
- [18] Waqas H., Qureshi A.H. Influence of pH on nanosized Mn–Zn ferrite synthesized by sol-gel auto combustion process. *J. of Thermal Analysis and Calorimetry*, 2009, **98**, 355.
- [19] Tugova E., Yastrebov S., Karpov O., Smith R., NdFeO₃ nanocrystals under glycine nitrate combustion formation. *J. of Crystal Growth*, 2017, **467**, P. 88–92.
- [20] Martinson K.D., Kozyritskaya S.S., Pantelev I.B., Popkov V.I. Low coercivity microwave ceramics based on LiZnMn ferrite synthesized via glycine-nitrate combustion. *Nanosystems: Physics, Chemistry, Mathematics*, 2019, **10**, P. 313–317.
- [21] Varma A., Mukasyan A.S., Rogachev A.S., Manukyan K.V. Solution combustion synthesis of nanoscale materials. *Chemical Reviews*, 2016, **116**, P. 14493–14586.
- [22] Dippong T., Levei E.A., Cadar O. Recent Advances in Synthesis and Applications of MFe₂O₄ (M = Co, Cu, Mn, Ni, Zn) nanoparticles. *Nanomaterials*, 2021, **11**, 1560.
- [23] Novitskaya E., Kelly J.P., Bhaduri S., Graeve O.A. A review of solution combustion synthesis: an analysis of parameters controlling powder characteristics. *International Materials Reviews*, 2018, **66**, P. 188–214.
- [24] Sutka A., Mezinskis G. Sol-gel auto-combustion synthesis of spinel-type ferrite nanomaterials. *Frontiers of Materials Science*, 2012, **6**, P. 128–141.
- [25] Chavarriaga E.A., Lopera A.A., et al. Gel combustion synthesis and magnetic properties of CoFe₂O₄, ZnFe₂O₄, and MgFe₂O₄ using 6-aminohexanoic acid as a new fuel. *J. of Magnetism and Magnetic Materials*, 2020, **497**, 166054.
- [26] Popkov V.I., Martinson K.D., et al. SCS-assisted production of EuFeO₃ core-shell nanoparticles: formation process, structural features and magnetic behavior. *J. of Alloys and Compounds*, 2021, **859**, 157812.
- [27] Martinson K.D., Kondrashkova I.S., et al. Magnetically recoverable catalyst based on porous nanocrystalline HoFeO₃ for process of n-hexane conversion. *Advanced Powder Technology*, 2020, **31**, P. 402–408.
- [28] Jadhav L.D., Patil S.P., Jamale A.P., Chavan A.U. Solution combustion synthesis: role of oxidant to fuel ratio on powder properties. *Materials Science Forum*, 2013, **757**, P. 85–98.
- [29] Chandra T., Ionescu M., Mantovani D. Structure and magnetic properties of Mn–Zn ferrite synthesized by glycine-nitrate auto-combustion process. *Advanced Materials Research*, 2011, **409**, P. 520–525.
- [30] Albadi A., Ivanova M.S., et al. The influence of co-precipitation technique on the structure, morphology and dual-modal proton relaxivity of GdFeO₃ nanoparticles. *Inorganics*, 2021, **9**, 39.
- [31] Sumathi S., Nehru M., Synthesis, characterization, and influence of fuel on dielectric and magnetic properties of cobalt ferrite nanoparticles. *J. of Superconductivity and Novel Magnetism*, 2016, **29**, P. 1317–1323.